




Mutual Interference of Automotive OFDM Radars—Analysis and Countermeasures

BENEDIKT SCHWEIZER  (Graduate Student Member, IEEE),
CHRISTINA KNILL  (Graduate Student Member, IEEE),
DAVID WERBUNAT  (Graduate Student Member, IEEE), **SIMON STEPHANY,**
AND CHRISTIAN WALDSCHMIDT  (Senior Member, IEEE)

(Regular Paper)

Institute of Microwave Engineering, Ulm University, 89081 Ulm, Germany

CORRESPONDING AUTHOR: B. Schweizer (e-mail: bschweizer@ieee.org).

This work was supported by the German Federal Ministry of Education and Research within the project IMIKO-Radar under Grant 16EMO0345.

ABSTRACT Due to its noise-like signal property, digital orthogonal frequency-division multiplexing (OFDM) radars are often assumed to be robust against interference. While a lot of research has been carried out for interference between different modulation schemes, the mechanisms of interference from OFDM to OFDM radars have been barely addressed. This paper provides a thorough analysis of mutual OFDM to OFDM interference based on radar measurements using a 4x4 77 GHz multiple-input multiple-output (MIMO) OFDM radar prototype. The effects of interference are described both qualitatively and quantitatively for cyclic-prefix and stepped-carrier OFDM. Second, it is shown that conventional mitigation methods in the spectrogram are not suitable due to the random coding of cyclic-prefix OFDM. As an alternative, the application of adaptive beamforming is proposed and two realization possibilities are provided. Finally, new mitigation strategies in the modulation domain are proposed. They allow to shape interference to specific range-Doppler cells, yielding an interference-free range-velocity map for the area of interest. Additionally, the method may be used as the basis to enable simple conventional interference mitigation strategies.

INDEX TERMS Automotive radar, beamforming, digital modulation, interference, millimeter-waves, MIMO, OFDM, radar systems, RF system-on-chip.

I. INTRODUCTION

Radar has an outstanding role in automotive safety and driving assistance systems due to its robustness to harsh weather conditions and the ability to measure distances and relative velocities. With the current development towards autonomous driving, the number of sensors per vehicle is expected to grow significantly. Additionally, future sensors will require larger bandwidths, longer frame durations, and higher frame repetition rates [1]. Since the available spectrum needs to be shared among all participants, interference will limit the performance of radar sensors.

At the same time, digital centric modulation schemes attract more and more attention. This process is driven by multiple factors. Ever-increasing demands on the abilities of the radars on resolution and unambiguously measurable

ranges push the established radars to their inherent limitations given by the analog hardware and frequency ramp generation. Recent complementary metal-oxide-semiconductor (CMOS) technologies on the other hand allow for the first time to realize digital-centric radar designs on chip, shifting the effort to the digital domain. This is partly driven by 5G developments in similar frequency bands requiring similar hardware. A last driving factor lies in the hope that digital modulation schemes can handle the interference threat by application of coding and correlation techniques.

So far, the research mainly focuses on interference between digital and analog radar sensors. The influence of a chirp-sequence frequency-modulated continuous-wave (FMCW) radar on an orthogonal frequency-division multiplexing (OFDM) radar is studied intensively in [2]. It is

shown that the instantaneously narrowband chirp signal is easily detectable in the wideband OFDM frame and the interfering energy can be removed by simple methods. These include the removal of the interfered cells in the spectrogram (zeroing) or energy leveling in the same domain. Furthermore, compressed-sensing techniques can be used to estimate missing signal parts [3], [4], and signal repairment based on linear prediction is possible [5]. In [6] the interference from OFDM to FMCW is studied theoretically with the conclusion that OFDM interference on chirp-sequence radars can be regarded as additional noise. A broad overview of automotive radar interference including a summary on mitigation possibilities is presented in [7]. Simulation-based comparative studies about which modulation scheme is more robust against interference have been performed in [8] and on a multi-frame base in [9] revealing that the fluctuations in the noise floor are smaller for OFDM radars. Yet, they do not include any clear analysis, nor provide countermeasures. In recent publications, a trend towards cooperative interference mitigation and avoidance is observable [10]–[12]. To be emphasized is the approach in [10]. The authors propose a cooperative concept based on pilot tones such that the interfering signal can be decoded and subtracted from the received signal. This may be considered as the best possible solution.

However, the influence of OFDM to OFDM interference is barely studied yet, and literature still lacks of simple and efficient countermeasures for such interference.

In this paper, mutual OFDM to OFDM interference is studied analytically and experimentally based on radar measurements. In contrast to FMCW radar waveforms, OFDM signals are instantaneously wideband due to the subcarrier structure. This applies to the radio frequency (RF) and baseband signal. It is shown that this property results in a different interference behavior compared to FMCW radars and the need for new compensation strategies, eventually leading to a suitable mitigation and prevention concept with minimal requirements on the waveform design.

The paper is organized as follows. In Chapter II, the signal model of cyclic-prefix OFDM is described, and the sampling-rate efficient variant stepped-carrier OFDM is introduced. A short description of the experimental radar system and measurement setup is given in Chapter III as it is used throughout the paper. Chapter IV and Chapter V describe and quantize the effects of interference followed by mitigation strategies in Chapter VI. It is shown that conventional mitigation techniques as used in [2], [4] are not applicable. Therefore, the use of adaptive digital beamforming is proposed, and two implementations based on reference signal generation and constant modulus algorithm (CMA) are given in Chapter VI-B as a universal mitigation method. Chapter VI-C proposes a new mitigation method in modulation domain. Based on repeated-symbol modulation, it is possible to shape the interference to arbitrarily selectable cells in the rv -map, while the rest is unaffected by interference. Based on the desired level of cooperation, the concept can be extended to a simple but efficient interference prevention strategy. Alternatively, it offers the

chance to apply classical mitigation strategies when used in a non-cooperative variant as described in Chapter VI-D. The modulation-domain mitigation strategy is further evaluated in presence of phase noise and timing offsets. All concepts are verified by radar measurements at 77 GHz throughout the paper, before the paper is concluded in Chapter VII.

A. NOTATION

Bold letters refer to vectors, underlined bold letters to matrices. Lower-case and upper-case letters refer to time and frequency domain, respectively. $(\cdot)^H$ is the complex-conjugate transposed, $(\cdot)^*$ is the complex-conjugate. \oslash indicates Hadamard-Division or point-wise division. $|\cdot|$ is the element-wise absolute value.

II. OFDM SIGNAL MODEL

A. CYCLIC-PREFIX OFDM

An OFDM frame consists of M OFDM symbols. Each such OFDM symbol of duration T consists of N continuous waves at frequencies $f_n = n\Delta f$. These so-called subcarriers are orthogonal due to the appropriate choice of the OFDM symbol duration $T = 1/\Delta f$. To avoid inter-symbol interference (ISI) a cyclic-prefix of duration T_{cp} is required before each OFDM symbol, increasing the total OFDM symbol duration to $T_{sym} = T + T_{cp}$. This scheme is further referred to as cyclic-prefix OFDM (CP-OFDM) [13] and described by

$$x(t) = \sum_{m=0}^{M-1} \sum_{n=0}^{N-1} d(n, m) e^{j2\pi n\Delta f t} \text{rect}\left(\frac{t - mT_{sym}}{T}\right). \quad (1)$$

For a standard OFDM frame it is assumed that the set of phase codes $d(n, m)$ is unique for each OFDM symbol m , such that a random coding is achieved for all modulation symbols in time and subcarrier dimension. The choice of the complex-valued phase codes $d(n, m)$ can be arbitrary and does not influence the radar performance directly. Common choices are quadrature phase-shift keying (Q-PSK) or random PSK. This degree of freedom allows to optimize the resulting waveform regarding signal properties such as the peak-to-average power ratio (PAPR) [14], [15].

The discrete-time baseband transmit signal $x(t)$ is realized digitally by an inverse discrete Fourier transform (IDFT) of the modulation symbols. For transmission it is converted to the RF band by a homodyne analog frontend. After reception of the reflected signal, it is amplified by a low noise amplifier (LNA) and converted to baseband, where it is sampled with a sufficiently high sampling rate after low pass filtering.

The Rx signal is evaluated in frequency domain. First, the transmitted modulation symbols $d(n, m)$ are removed by a spectral division, and the range and Doppler information is extracted by an IDFT and DFT, respectively.

B. STEPPED-CARRIER OFDM

Additionally, the stepped-carrier OFDM modulation scheme (SC-OFDM) is investigated [16]. It can be considered as an enabler for wideband digital radars since the requirements on

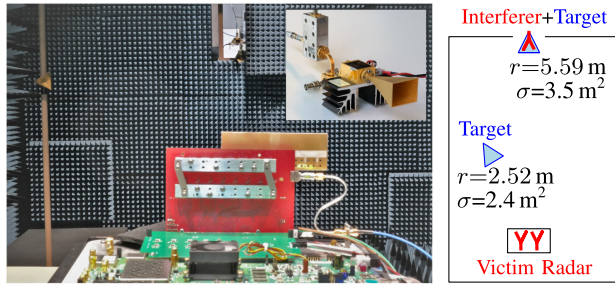


FIGURE 1. Photographs and drawing of the measurement setup. The victim radar consists of an RFSoc as digital backend that is connected to the radar front end. The interfering radar (picture-in-picture) is placed in the window on the opposite side of the anechoic chamber. The targets are realized with two corner reflectors. One target is co-located with the interfering radar.

sampling rates and processing capabilities are reduced. Compared to CP-OFDM it utilizes a small-bandwidth OFDM baseband signal with fewer subcarriers, that is converted to RF-domain with an agile carrier. The carrier frequency is changed by integer multiples of the baseband bandwidth B_{baseband} after each OFDM symbol. In this way, the bandwidth of an equivalent CP-OFDM symbol B_{channel} is generated artificially using $M_{\text{step}} = B_{\text{channel}}/B_{\text{baseband}}$ steps. The actual step pattern can be arbitrary, i.e. linear

$$f_c(m) = f_{c,0} + (m \bmod M_{\text{step}})N\Delta f \quad (2)$$

or any other permutation of the required steps.

III. MEASUREMENT SETUP

To verify the interference effects and mitigation methods, an experimental digital radar system is used as the victim [17]. It consists of an RF system-on-chip (RFSoc) with integrated high-speed data converters to generate and sample the transmit (Tx) and receive (Rx) baseband signals [18]. This backend is connected to an analog frontend that utilizes eight single channel transmit-receive (TRx) monolithic microwave integrated circuits (MMICs) at 77 GHz [19]. To minimize the Tx-Rx leakage, four MMICs are used as Tx and Rx, respectively. The tapered series-fed patch antenna arrays have a gain of 12 dBi [20]. The interfering radar is realized with an experimental radar system in waveguide technology [16]. The interference signal is generated with an arbitrary waveform generator (AWG) and converted to 77 GHz. It is amplified and transmitted by a standard gain horn with $G=25$ dBi. The equivalent isotropically radiated power (EIRP) of the RFSoc radar is around 4 dBm, and the EIRP of the interfering radar is around 10 dBm.

The measurement scene consists of two corner reflectors at 2.52 m and 5.59 m at different azimuth angles. The interfering radar is placed at 5.59 m as well. The scene and both radar systems are shown in Fig. 1. All relevant modulation parameters are given in Table 1.

TABLE 1. Parameters of Victim OFDM Radar and Interferer, If Not Noted Otherwise.

Radars	Victim		Interferer	
Steps M_{step}	1	4	1	4
Subcarriers N_c	2048	512	800	400
Subcarrier spacing Δf (kHz)	200			
Bandwidth B (MHz)	410		160	320
OFDM symbols M	2048		> 2048	
Duration of cyclic-prefix T_{cp} (μs)	0.5		0	0.5
Transmit power P_{Tx} (dBm)	−8		−15	
Antenna gain $G_{\text{Tx/Rx}}$ (dBi)	12		25	

IV. INTERFERENCE ANALYSIS

In this chapter the interference of OFDM radars and the effects during evaluation are described for CP-OFDM and SC-OFDM.

A. INTERFERENCE OF CP-OFDM RADARS

In contrast to classical, frequency modulated modulation schemes, the most relevant differences in terms of interference analysis are the continuous-wave (CW) carrier, the coding, and the large signal bandwidth $B=N\Delta f$, which is the same in baseband and at the RF. Due to the constant carrier frequency and the digital nature of the signal, any interference is straightforwardly converted to baseband without any modification. This allows to clearly identify any interference. Due to the large signal bandwidth, the probability of an interfering signal being present within the RF-band is significantly larger than for an FMCW signal.

The starting point for the interference analysis can be broken down to the following scenario: The victim radar observes the channel with bandwidth B_{obs} for the duration T_{obs} . Any undesired signal in this time-frequency frame can be considered as interference. The impact of an OFDM interferer depends on the relative overlap O_{time} and O_{freq} of the observation frames of both radars in time and frequency, and the standard parameters distance of the interferer $R^{(i)}$, antenna gains $G_{\text{Tx}}^{(i)}$ of interferer and $G_{\text{Rx}}^{(v)}$ of the victim, and the transmit power of the interferer $P_{\text{Tx}}^{(i)}$. The indices (i) and (v) indicate interferer and victim, respectively. The energy contribution by interference at the victim radar is

$$E_{\text{Rx}}^{(i)} = \frac{P_{\text{T}}^{(i)} G_{\text{T}}^{(i)} G_{\text{R}}^{(v)} \lambda^2}{(4\pi R^{(i)})^2} O_{\text{time}} O_{\text{freq}} T_{\text{obs}}^{(v)}. \quad (3)$$

In the following, it is shown how the interference manifests itself during the different evaluation steps. The corresponding measurement examples are given in Fig. 2. The columns refer to different types of modulations, and the rows correspond to the evaluation steps.

1) TIME-DOMAIN SIGNAL

After conversion to baseband the time-domain signal is the superposition of two signals, the received radar signal and the

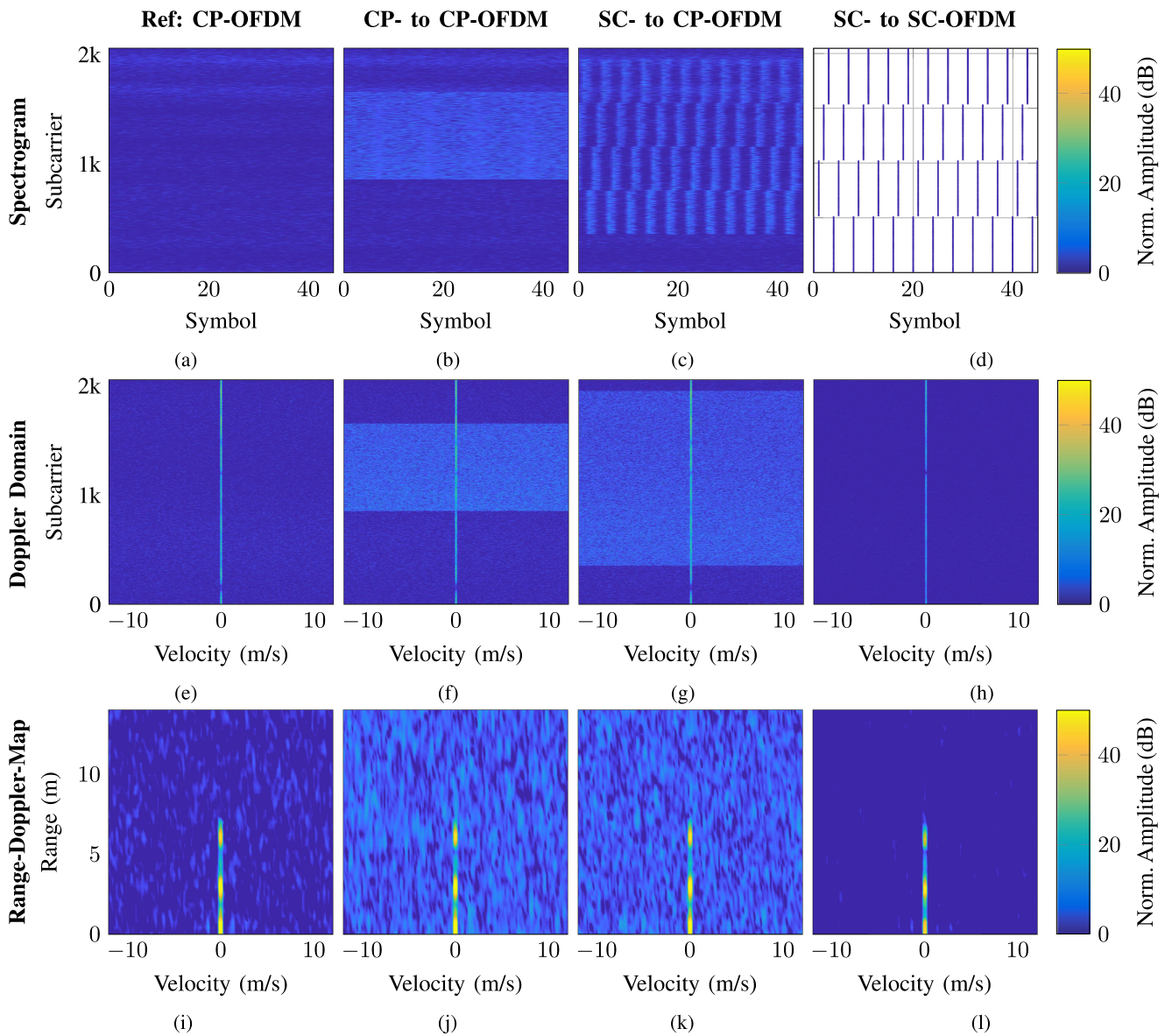


FIGURE 2. Measurements of OFDM to OFDM interference. The rows show the spectrogram, Doppler, and range-Doppler estimation corresponding to the necessary processing steps. Column 1: CP-OFDM reference measurement without interference. Column 2: Interference from CP-OFDM to CP-OFDM. Column 3: Interference from SC-OFDM to CP-OFDM. Column 4: Interference from SC-OFDM to SC-OFDM.

interference. Since both signals are noise-like, they cannot be distinguished directly, especially for weak interferers.

However, calculating a mean power for small time frames may allow to determine the presence of an interferer. This corresponds to a classical energy detection approach [21]. Due to the wideband structure of both signals, interference is present for a long duration such that any mitigation in this domain is not promising.

2) SPECTROGRAM

Since the evaluation of OFDM signals is performed in frequency domain, a DFT is applied on the time-domain signal of each OFDM symbol, leading to a spectrogram. During this step interference is concentrated to those modulation symbols

$d(n, m)$ in the spectrogram that are interfered. This allows a first precise estimate of the interfering signal to characterize its bandwidth, carrier frequency, and measurement duration. An exemplary spectrogram of the first OFDM symbols of an interfered frame is given in Fig. 2(b) compared to a reference without interference in Fig. 2(a). The interferer affects around 800 subcarriers for the whole frame duration with a power spectral density that is around 8.5 dB larger than the OFDM signal for the Rx channel in this example.

As an initial processing step to allow range-Doppler-evaluation, an element-wise spectral division by the Tx modulation symbols is applied in this domain [22], [23]. This causes the interference to be de-correlated due to the random coding of CP-OFDM [24].

3) DOPPLER ESTIMATION

Applying a DFT on the modulation symbols along time compresses the signal energy into the corresponding velocity bin, as shown in Fig. 2(e) for stationary targets. In case of CP-OFDM interference, c.f. Fig. 2(f), the interfering energy affects the same subcarriers but is eventually distributed over all velocity bins. Since the DFT is a linear operation, the target energy is still compressed to the corresponding Doppler bin.

4) RANGE-DOPPLER ESTIMATION

The energy of target reflections is concentrated in the corresponding range-velocity cell with a processing gain of $G_p=MN$ in total. Since interference signals do not sum up coherently due to the de-correlation by the spectral division, their energy is spread over the whole rv -map as shown in Fig. 2(j). The resulting interference noise level is

$$P_{RV}^{(i)} = \frac{E_{Rx}^{(i)}}{MN}. \quad (4)$$

B. INTERFERENCE OF STEPPED-CARRIER OFDM RADARS

In principle, the general analysis holds true for SC-OFDM radars as this scheme is only an extension of the CP-OFDM scheme. Minor differences occur due to the partial usage of the channel that can be included in the overlap coefficients. The special peculiarities of SC-OFDM to CP-OFDM and SC-OFDM to SC-OFDM interference are highlighted in the following.

1) SC-OFDM TO CP-OFDM INTERFERENCE

In the case of an SC-OFDM interferer and a wideband CP-OFDM victim, the result is similar to CP-OFDM to CP-OFDM interference. The transmit power is limited by the power amplifier (PA) in both cases, such that the total energy of the SC-OFDM interferer is equal to the standard OFDM radar. Although the stepping pattern is clearly visible in the spectrogram (Fig. 2(c)), the energy is distributed throughout the rv -map (Fig. 2(k)) during evaluation, leading to a similar noise floor as in Fig. 2(j).

2) SC-OFDM TO SC-OFDM INTERFERENCE

For two SC-OFDM radars, the situation may differ for specific setups. Depending on the stepping pattern and the symbol duration, the relative overlap in time-frequency domain may vary between 0 and 1. This has immediate consequences on the resulting SNR. The last column in Fig. 2 presents the results for SC-OFDM to SC-OFDM interference for a measurement with relatively low overlap. The resulting rv -map is barely affected by interference.

In general, the severity of interference between SC-OFDM radars is a result of the stepping patterns. Assuming the same symbol duration T_{sym} , perfect synchronization and $M_{step}=4$ steps, the combination of the stepping patterns has a direct impact on the performance. With a probability of 33,3 %, one step position is interfered, in 25 % of all cases, two step positions are interfered and the chance for identical patterns

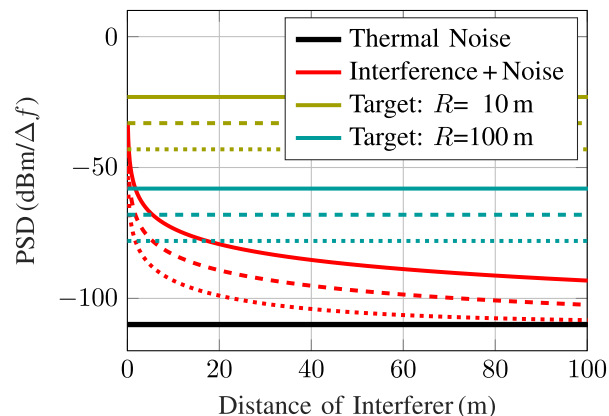


FIGURE 3. Influence of interference on detection capabilities vs. distance of the interferer. Solid, dashed, and dotted lines refer to a mean transmit power of 20 dBm, 10 dBm, and 0 dBm, respectively, for both interferer and radar. The two sets of horizontal lines refer to the processed Rx power of target reflections for targets with an RCS value of 10 dBsm at distances of 10 m, and 100 m.

associated with maximum interference is 4.2%. The probability of interference-free operation is still 37.5 %.

However, if both radars choose their subcarrier spacing and cyclic-prefix duration arbitrarily, the stepping pattern has a minor influence. Throughout one frame, all step positions are affected periodically, leading to an averaging effect. The expected value of the interference noise floor is a few dB below that of CP-OFDM interference. Yet, the stepping pattern can be exploited to allow simultaneous usage of the channel by multiple radars [11].

V. QUANTITATIVE ANALYSIS

The interference-induced noise level is limiting the performance, if it is larger than the intrinsic thermal noise floor of $PSD_{noise}=k_B T \Delta f (B_{LP}/f_s) F$ that depends on the subcarrier spacing, the bandwidth of the low pass filter B_{LP} , the sampling rate f_s , the noise factor F , the Boltzmann constant k_B , and the temperature T . This behavior is displayed in Fig. 3 for $\Delta f=500$ kHz, $N=M=2048$, $F=5.01$, $B_{LP}=f_s$, and $T=290$ K. In addition to the thermal noise level at -110 dBm/500 kHz, the resulting noise levels in case of an interferer are given in dependency of the distance of the interferer for three different Tx power levels of 20 dBm, 10 dBm, and 0 dBm. Interference has the strongest influence if the distance is small, i.e. below 10 m. To visualize the impact on the detectability of targets, the resulting power level for a target at 10 m and 100 m in the rv -map is given for the same Tx powers of 20 dBm, 10 dBm, and 0 dBm. Based on this graph the detection performance of the victim radar can be estimated depending on the distance of the interferer. The loss in SNR is readable from the distance between the thermal noise floor and the interference-induced noise level.

Fig. 4 analyzes the maximum achievable range depending on the interferer's distance assuming the same EIRP for both radars. The nearer the interferer, the smaller is the maximum

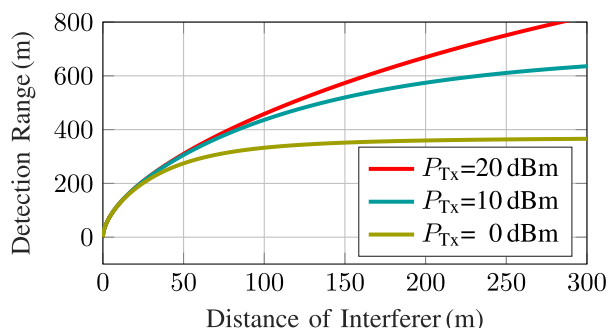


FIGURE 4. Maximum detection range for $P_{Tx}=(20, 10, 0)$ dBm (equal for victim and interferer). The target has an RCS of $\sigma = 10$ dBsm and the radar parameters are given in Table 1. A target is considered detectable for $SNR > 12$ dB.

detection range. This is severe especially for small distances below 10 m, where the maximum range goes below 120 m. In this region the EIRP does not contribute to the detection performance, as long as it is the same for both radars. This analysis allows the following conclusions: Interference by OFDM radars is especially severe for interferers in small distance. This can be a passing car or a car driving in front with a back-looking radar used for blind spot detection or lane change assist. Although the effect of both scenarios is very similar, the way how to deal with them varies drastically: While the oncoming car passes the victim radar quickly, the passing car and the one driving in front may stay there for a long duration. For the oncoming car, there is a small probability that both radars operate in the same time frame during the short time slot where they are within that close proximity to each other. However, the probability of severe interference is drastically higher for the car driving in the same direction. Based upon this observation, suitable mitigation methods are developed in the following.

VI. INTERFERENCE MITIGATION

A. EVALUATION OF CONVENTIONAL MITIGATION METHODS

The term conventional mitigation is used to describe signal processing methods that manipulate the interfered Rx signal such that the effect of the disturbance is minimized. The goal of all mitigation techniques is to reduce the energy contribution of the interferer to the final rv -map in order to maximize the dynamic range. This should be achieved without limiting the performance of the radar in any other domain and without generating ghost targets or artifacts. Interference mitigation may be applied during any of the required processing steps, from sampled time-domain signal to rv -map. The suitability of a domain depends the modulation scheme, the interfering signal, performance requirements, and available processing capabilities. In general, a domain is suitable for interference detection and mitigation, if the interfering energy is concentrated to some samples with a clear effect on the magnitude.

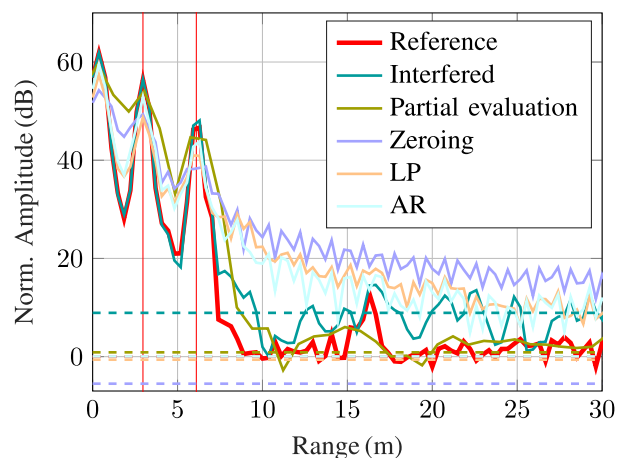


FIGURE 5. Comparison of conventional mitigation methods (zeroing, amplitude rescaling (AR), linear prediction (LP)) being applied on the measurements of CP-OFDM to CP-OFDM interference according to the measurement setup in Fig. 1. (—): Range profiles for $v = 0$. (---): Corresponding noise level in the rv -map. (|): Ground truth of targets. The amplitude is normalized to the noise level of the reference measurement.

This can be the time domain for FMCW to FMCW interference [25]–[27] or the spectrogram for FMCW to OFDM interference. For the latter, the energy gets compressed to only a few modulation symbols that can easily be zeroed out or reconstructed [2]. As analyzed in the previous chapter, OFDM interference is a wideband, noise-like signal and it remains noise during the evaluation, where it is eventually spread over the complete rv -map. In terms of interference mitigation, this is a drawback of the OFDM modulation. Although it is simple to detect and characterize interference, it is hard to apply conventional mitigation techniques due to the noisy characteristics of the interfering signal. There is no domain in which the interfering energy is compressed to a few samples, thus interference mitigation is challenging.

This is demonstrated in Fig. 5 for the CP-OFDM to CP-OFDM interference from Fig. 2(j). The conventional mitigation techniques for OFDM radars are applied on the spectrogram. The interfered area is determined based on amplitude thresholding and the interfered cells are mitigated using zeroing,¹ amplitude rescaling,² interpolation based on linear prediction, and partial evaluation of the larger band of sub-carriers that have not been affected by interference. Although all methods reduce the interference induced noise floor to the level of thermal noise, it can be seen that none of the methods zeroing, amplitude rescaling, and interpolation lead to an improved rv -map, since the interfered area still causes a strong sinc-pattern in range direction. Only the partial evaluation leads to an acceptable rv -map at the cost of a reduced range resolution.

¹Zeroing: The amplitude of the interfered cell is set to zero.

²Amplitude rescaling: The amplitude of the interfered cells is reduced to the amplitude without interference based on signal statistics to reduce the rectangular amplitude pattern.

1) DISCUSSION

This leads to the conclusion that conventional interference mitigation is not applicable for OFDM to OFDM interference. Thus, the ideal solution is to avoid interference per design. Yet this would impose strict regulations that all radars had to obey making this approach impractical. In the following, suitable alternatives are presented.

For the oncoming car, it might be sufficient to mitigate the interference and accept performance degradation of a small percentage of all frames. A suitable and well-known method to handle this interference is beamforming.

For the long-duration, high probability interference from the car driving in the same direction, such a method is not applicable, since the performance is limited for a long duration. Therefore, a new method in modulation domain is proposed.

B. ADAPTIVE DIGITAL BEAMFORMING

Digital beamforming [28] is a well-known technique to steer the transmit or receive beam of an antenna array in a specific angular direction. Steering of the Rx beam is achieved with a weighted summation of all Rx channels such that the individual Rx signals interfere destructively for the angle that should be suppressed. If the direction of the interferer is known, the weights can be set directly using a classical beamforming technique [29], [30]. However, especially in automotive applications, the scenarios are non-stationary, and the existence and position of an interferer changes rapidly. Therefore, adaptive beamforming algorithms that determine the required weights during operation are advantageous.

In the following, two suitable adaptive beamforming algorithms and their integration into the OFDM signal processing chain are presented.

1) LEAST-SQUARES METHOD

A low-complexity algorithm for adaptive beamforming is based on the least squares method (LSM) [31]. It is applied on the sampled time-domain Rx signal x_{Rx} . For the k -th iteration, the k -th samples of all P Rx antennas are combined in the vector $\mathbf{x}(k)$. The optimization goal is to determine the weight vector \mathbf{w} such that the deviation $e(k)$ of the output signal $y(k)=\mathbf{w}^H(k)\cdot\mathbf{x}(k)$ compared to an interference-free reference signal $z(k)$ is minimized. This error $e(k)$ is

$$e(k) = z(k) - \mathbf{w}^H(k) \cdot \mathbf{x}(k). \quad (5)$$

The weight vector is updated recursively according to

$$\mathbf{w}(k+1) = \mathbf{w}(k) + \xi e^*(k) \cdot \mathbf{x}(k), \quad (6)$$

with an update coefficient ξ . Thereafter, the usual processing steps are applied on $y(t)$ to obtain one rv -map.

For chirp-sequence radars a non-interfered segment of the time-domain Rx signal suits as the reference [32]. Due to the wideband and time-continuous interference and symbol-wise CP-OFDM structure with unique phase codes, this concept is not applicable for OFDM radars. Instead, the reference signal can be constructed as follows: First, the range-velocity evaluation is performed for each virtual channel despite interference.

Based on a non-coherent integration of all virtual rv -maps, a single rv -map is obtained. Although it suffers from low SNR due to the interference, it is to expect that the Tx-Rx leakage and strong targets are still visible. The reference signal is generated by thresholding the rv -map and setting all values below the threshold to zero such that a noise-free rv -map with only the leakage and strong targets is present. Afterwards, the whole rv processing chain is rewound in reverse order (FFT along range, IFFT along velocity, spectral multiplication with phase codes, IFFT along subcarriers) to obtain the final reference signal in time domain. This signal, that is the noise- and interference-free Rx signal for the strongest targets, works well as a reference.

2) CONSTANT MODULUS ALGORITHM

To avoid the costly calculation of a reference signal, algorithms that do not require a reference signal are advantageous. The constant modulus algorithm (CMA) [33] in frequency domain is able to determine the weight vector based on the assumption that the spectrum of the received signal has a constant modulus, i.e., the spectrum is flat. This property is violated by interference.

The recursive algorithm [34], [35] can be included into the signal processing chain of the Rx OFDM symbols. In the spectrogram and after the spectral division, the N received modulation symbols of the m -th OFDM symbol $\mathbf{d}_{\text{RX}}(m) \in \mathbb{C}^N$ of all P Rx channels form the input matrix $\mathbf{X}(m) \in \mathbb{C}^{P \times N}$ of iteration m . Based on the weight vector of the previous iteration, the output signal

$$\mathbf{Y}(m) = \mathbf{w}^H \cdot \mathbf{X}(m), \quad \mathbf{Y}(m) \in \mathbb{C}^{1 \times N} \quad (7)$$

is a vector of modulation symbols being the weighted sum of all receive channels. $\mathbf{Y}(m)$ is used for further rv -evaluation.

At the same time, the error \mathbf{E} is determined as

$$\mathbf{E}(m) = \mathbf{Y}(m) \otimes |\mathbf{Y}(m)| - \mathbf{Y}(m), \quad (8)$$

that is used to update the weight vector

$$\mathbf{w}(m+1) = \mathbf{w}(m) + \xi \mathbf{X}(m) \cdot \mathbf{E}^H(m) \quad (9)$$

with an update coefficient ξ . It should be noted that the spectrum is not flat in case of multiple targets. However, the violation by the strong interferer is much more severe than any target-induced amplitude variation. Thus, the algorithm is able to notch out this disturbance at first. If there are more Rx antennas available, it might be helpful to use a setup that only allows to place as many zeros as there are interferers. The approach might fail, if the interferer covers the full bandwidth of the radar.

3) MEASUREMENT EVALUATION AND DISCUSSION

Fig. 6 compares the resulting range profiles after the application of LSM and CMA with non-coherently integrated range profiles of an interference-free reference measurement and the interfered measurement. Both algorithms have a similar performance. It is possible to achieve an SNR of 56.5 dB (CMA) and 55.5 dB (LMS) for the target at $r=3$ m. This matches the

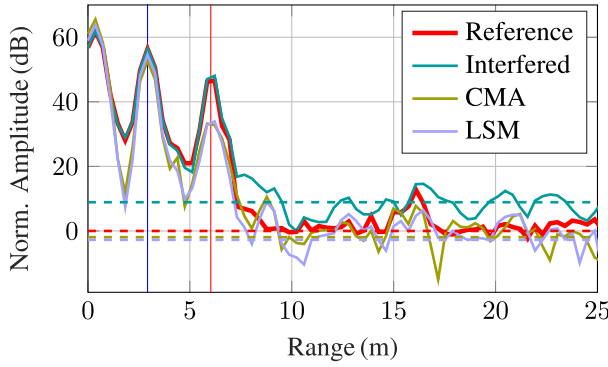


FIGURE 6. Adaptive beamforming. (—): Measured range profiles for reference without interference, interfered measurement, and after beamforming with LSM and CMA. (---): Corresponding noise level in *rv*-map. (|): Ground truth of target at 2.52 m. (|): Ground truth of target co-located with interferer at 5.59 m. All curves normalized to noise level of reference measurement.

SNR of 56.4 dB obtained by the non-coherent integration of the reference measurement. Since the interferer at $\theta^{(i)}=0^\circ$ is notched out, the target at $r=6.07$ m with similar angle is strongly attenuated,³ and also far-away targets behind the interferer in the same angular direction are removed (target at $r=16$ m).

C. COOPERATIVE MITIGATION IN MODULATION DOMAIN

As analyzed in Chapter VI, OFDM interference is a noise-like signal such that any mitigation is challenging. As a consequence, alternative modulation and evaluation schemes are required that are able to compress the interfering energy in a specific domain such that detection and mitigation is simplified. The solution is to use the repeated-symbol OFDM (RS-OFDM) scheme [36] in both radars.

1) MATHEMATICAL MODEL

Similar to the description of CP-OFDM (1) in Chapter II, the RS-OFDM frame consists of M OFDM symbols. However, instead of using a unique set of phase codes $d(n, m)$ for each OFDM symbol, one OFDM symbol with phase codes $d(n)$ is repeated throughout the frame without a cyclic-prefix. The interfering radar transmits such a RS-OFDM signal

$$x_{Tx}^{(i)}(t) = \sum_{m=0}^{M-1} \sum_{n=0}^{N-1} d^{(i)}(n) e^{j2\pi(f_c^{(i)} + n\Delta f)t} \text{rect}\left(\frac{t-mT}{T}\right) \quad (10)$$

at carrier frequency $f_c^{(i)}$ with repeated symbol coding $d^{(i)}(n)$ and symbol duration $T=1/\Delta f$ without using a prefix. After reception by the victim, the signal is converted to baseband with carrier frequency $f_c^{(v)}$ resulting in

$$x_{Rx}^{(i)}(t) = \sum_{m=0}^{M-1} \sum_{n=0}^{N-1} d^{(i)}(n) e^{j2\pi[n\Delta f + (\delta f_c + f_D^{(i)})t - (n\Delta f + f_c^{(v)})\frac{R_0^{(i)}}{c_0}]}$$

³The target at $r=6.07$ m does not disappear completely, since there is clutter caused by the wall of the anechoic chamber in the same range cell.

$$\times \text{rect}((t-mT)/T), \quad (11)$$

with the difference between the carrier frequencies $\delta f_c = f_c^{(i)} - f_c^{(v)}$, the distance of the interfering radar $R_0^{(i)}$, and the one-way Doppler frequency $f_D^{(i)} = v^{(i)}(f_c^{(v)} + n\Delta f)/c_0$. It is assumed that the subcarrier spacings of both radars are equal. A partial overlap may be considered by setting the respective modulation symbols to zero. With the narrow-band assumption ($N^{(i)}\Delta f \ll f_c^{(i)}$) the resulting Rx modulation symbols after spectral division by the victim's Tx modulation symbols are given as

$$d_{div}^{(i)}(n, m) = \frac{d^{(i)}(n)}{d^{(v)}(n)} e^{-j2\pi(n\Delta f + f_c^{(v)})\frac{R_0^{(i)}}{c_0}} e^{j2\pi(\delta f + f_D^{(i)})mT} \quad (12)$$

$$= c(n) \cdot e^{j2\pi(\delta f + f_D^{(i)})mT}. \quad (13)$$

The first part indicated with $c(n)$ results in modulation symbols that depend solely on the respective subcarrier n . The distance of the interferer and the carrier frequency offset affect those modulation symbols, but this factor is *constant* over the OFDM symbols. The second part is induced by the relative velocity and carrier frequency offset between the interfering radar and the victim radar. This term depends on m , i. e., there is a phase progression over the OFDM symbols of the victim radar, which may be used to mitigate interference.

2) INTERFERENCE SHAPING IN MODULATION DOMAIN

If interference according to the description above is present, the Rx signal of the victim radar is the superposition of its own radar signal and the interference. Assuming the same subcarrier spacing Δf for both radars, the received modulation symbols of the victim radar $d_{div}^{(v)}(n, m)$ are the sum of the desired Rx modulation symbols of the victim $d_{div}^{(v)}(n, m)$ and those of the interferer (12), i. e.,

$$\begin{aligned} d_{div}(n, m) &= d_{div}^{(v)}(n, m) + d_{div}^{(i)}(n, m) \\ &= d_{div}^{(v)}(n, m) + c(n) e^{j2\pi(\delta f + f_D^{(i)})mT}. \end{aligned} \quad (14)$$

Due to the RS-OFDM coding, any interval of duration T can be processed correctly with the DFT, and both signals do not have to be synchronized. Only the phase of the received interferer's modulation symbol changes, but this constant offset does not influence the following processing steps.

During *rv*-processing the energy of the targets is compressed to the corresponding bins of the *rv*-map, since the desired modulation symbols $d_{div}^{(v)}(n, m)$ are not manipulated by the interference, similar to the description of CP-OFDM in Chapter IV-A3.

In contrast, the interference is not concentrated in range, since the modulation symbols $c(n)$ are de-correlated due to the spectral division by the *wrong* modulation symbols in (12). If the interference covered the victim's bandwidth only in parts, the interference is further spread to all range cells.

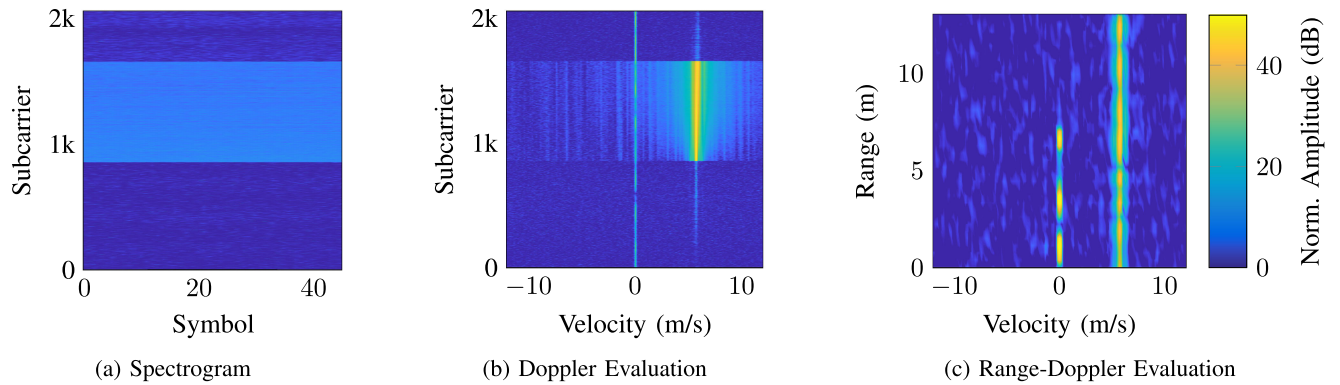


FIGURE 7. Mitigation in modulation domain using RS-OFDM based on measurements. The interference is compressed to one velocity column during evaluation.

For velocity estimation a DFT is applied on (14). The relevant part for the processing of the interference is (13), yielding

$$v^{(i)}[k] = \sum_{m=0}^{M-1} c(n) e^{j2\pi(\delta f + f_D^{(i)})mT} e^{-j2\pi mk/M} \quad (15)$$

with a maximum at velocity index $k = M(\delta f_c + f_D^{(i)})/\Delta f$.

This means that the interference is compressed to one velocity column in the rv -map due to the dependency on m in terms of a linear phase progression in the received modulation symbols of the interference. The index of this cell depends on the relative frequency offset between interferer and victim, i.e. on the carrier-frequency offset and the relative velocity. This enables to shift the interference to a velocity index that is not relevant during radar operation. The rest of the rv -map is unaffected, i.e., the noise floor and target peak shape are similar to the non-interfered case.

The measurement results in Fig. 7 show that the SNR is similar to the non-interfered case, and only the velocity index corresponding to $v = 5$ m/s has an increased noise level.⁴

To exploit the benefits of this scheme, the resulting interference ridge should be placed outside the actual area of interest. Common parameterizations of the OFDM modulation have a very large unambiguously measurable velocity due to the short symbol duration. Due to the loss of orthogonality caused by Doppler-shifts of the subcarriers, only 20% of the unambiguous area can be used in order to obey the criterion $f_{D,\max} < \Delta f/10$ [37]. This leaves a large portion of the rv -map for the interference to be placed without reducing the actual velocity domain. The most intuitive approach would be a shift by $\Delta f/2$ resulting in an interference ridge at the outermost velocity index.

Since the concept has minimal demands on the signal design (only RS coding), it can be implemented without specific cooperation or communication between the sensors. In the most simple case the victim radar may react on RS-OFDM

⁴Note that this index has been chosen on purpose to visualize the concept. This is not a desirable parameterization.

interference autonomously by shifting the interference to a suitable area. Since the victim radar modifies its transmit signal, the interferer benefits from this modification as well.

On a higher level it is possible to define general rules how to modify the Tx signal. As an example, the frequency shift may be chosen depending on the radar's mounting position on the vehicle. Alternatively, the frequency shift may depend on the global orientation of the radar sensor, i.e. on the cardinal direction with the sliding or discrete compass method [38]. This way, two sensors facing each other always shape the interference beneficially.

3) IMPLEMENTATION ASPECTS AND LIMITATIONS

The derivation above was performed for the ideal assumption of equal symbol durations and a constant carrier frequency offset. Since both radars have independent local oscillators, there is no phase relation between them such that the ideal assumption of a constant frequency offset is not fulfilled. Assuming oscillators with a frequency precision of 25 ppm, both 77 GHz frequency synthesizers may vary by up to 1.925 MHz, which is a multiple of the subcarrier spacing. Yet, the frequency deviation within one measurement frame is much smaller such that the carrier frequency spacing can be considered constant during one frame.

Phase noise, on the other hand, is uncorrelated between both radars. It appears as a random fluctuation of the instantaneous carrier frequency during the frame duration. As a consequence, the phase progression varies slightly from OFDM symbol to OFDM symbol, making it noisy. This leads to a smear in velocity direction, resulting in a couple of neighboring velocity bins being affected by interference. This is illustrated in Fig. 8 via simulations using a random walk phase noise model for the interfering radar [39], [40]. Both velocities are set to zero and the interference is shaped towards 10 m/s. The ideal simulation shows a clear concentration in one velocity column, whereas in the simulation including phase noise, the phase noise skirt can be recognized. This observation is well in accordance with the measurement result in Fig. 7(b).

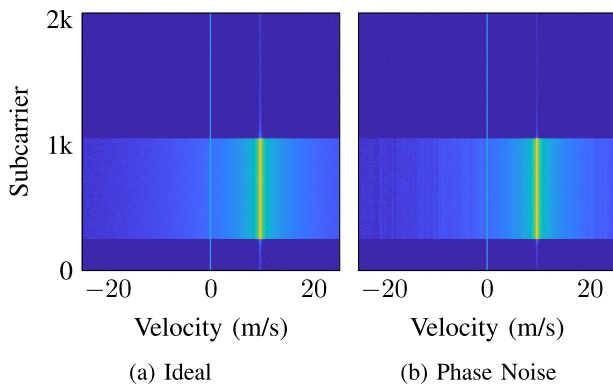


FIGURE 8. Simulated RS-OFDM to RS-OFDM interference. Effects of phase noise on interference shaping in Doppler-subcarrier domain. Normalized Amplitude (dB). Same scale as in Fig. 7.

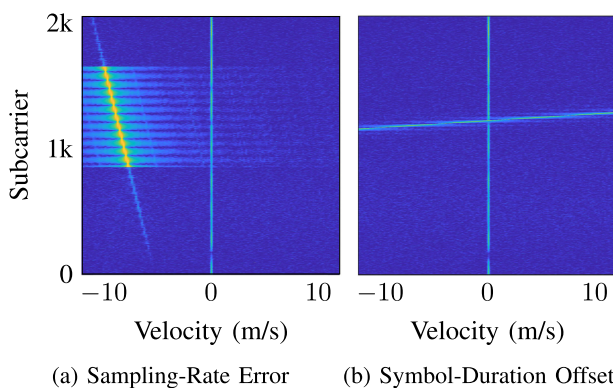


FIGURE 9. Measurements for RS-OFDM to RS-OFDM interference. Effects of differences in symbol duration T_{sym} in Doppler-subcarrier domain. (a): Oscillator-based sampling rate error. (b): Offset by $\Delta T_{\text{sym}} = 0.05\%$ by signal synthesis. Normalized Amplitude (dB). Same scale as in Fig. 7.

In case of symbol duration differences, the interfering OFDM symbol μ is not sampled coherently but with a small timing offset $\Delta T_0(\mu)$. This causes a phase progression over the OFDM symbols m . During Doppler evaluation the phase progression is estimated as a frequency and compressed to the corresponding Doppler bin. Since the phase progression is subcarrier dependent due to the increasing frequency $n\Delta f$, the frequency offset increases with the subcarrier index n . As a result, the interference is not concentrated in one velocity column but appears as a ramp in the spectrogram as shown in Fig. 9. The slope of the ramp decreases with increasing OFDM symbol duration difference.

4) DISCUSSION

The concept to shape the interference to one velocity column requires a precise tuning of the symbol durations and carrier frequency offset. Even small deviations lead to a large spread of the interference over multiple cells. However, this spread that occurs in the form of a ramp with its slope depending on the offset can again be used to estimate the offset iteratively in order to synchronize both radars. The digital signal generation

and evaluation principle offers best preconditions to realize the small carrier frequency offset. With the knowledge of the offset, the signal can easily be shifted to a digital IF-carrier frequency.

Finally, it is important to note that the concept not only mitigates OFDM to OFDM interference but can handle any interference signal that is repeated continuously. This includes phase-modulated continuous wave (PMCW) waveforms and also fast FMCW/chirp-sequence radars.

D. MITIGATION IN MODULATION AND DOPPLER DOMAIN

In addition to the interference-shaping method, that requires a minimum amount of cooperation between the sensors, the mitigation method in modulation domain can be used to mitigate interference in a more general way. This requires the symbol durations of both radars to be different, which is the default case. With this method, the interference is compressed to distributed peaks after Doppler evaluation, that may be mitigated using conventional interference mitigation methods.

The idea is linked to the analysis of different symbol durations in Chapter VI-C3. If the symbol duration offset between the sensors increases beyond the errors of the signal synthesizer, the slope of the ramp in Doppler-subcarrier domain decreases further. For large deviations it does not occur as a ramp but as a large number of small peaks in the Doppler domain, as shown in Fig. 10(a). The interference is concentrated to a few cells. This allows to detect and mitigate the affected cells before range estimation, such that the interfering energy is reduced drastically. The detection of the peaks is conveniently realized with a constant false alarm rate (CFAR) algorithm, and the conventional methods from Chapter VI-A can be applied to cancel the interference and even reconstruct the signal in order to optimize the final rv -map. As shown in Fig. 10(d), the resulting rv -map after zeroing the interfered cells in Fig. 10(b) is significantly improved in terms of SNR. Only small ridges close to the thermal noise floor remain due to the imperfect cancellation.

1) DISCUSSION

In contrast to the conventional mitigation methods, only a few contiguous subcarriers need to be mitigated. Such a small gap may be reconstructed much easier and with better results compared to a reconstruction in the spectrogram. Even if an interference peak occurs in a velocity column with targets being present, the method is still applicable. However, it should be noted that in such cases a reconstruction is favorable compared to zeroing to avoid having a sinc-pattern in the range profile of the corresponding velocity. Since the Doppler compression is already performed, the SNR of the range signal over the subcarriers is increased. This further improves the quality of the reconstruction. The most suitable reconstruction techniques in this context are linear prediction or compressed sensing.

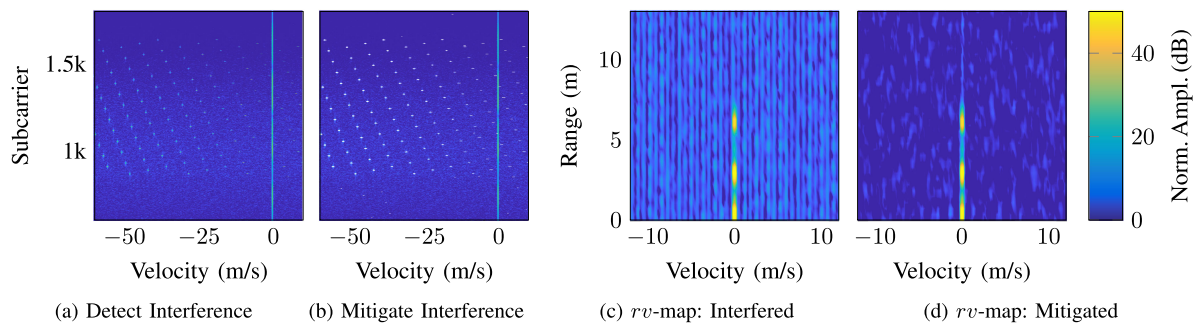


FIGURE 10. Non-cooperative interference mitigation in modulation domain and Doppler-subcarrier domain using RS-OFDM based on measurements: (a): The interference is compressed to many peaks in Doppler-subcarrier domain, which can be detected and zeroed (b). (c) rv -map of interfered measurement. (d) rv -map after zeroing the interference in Doppler-subcarrier domain.

VII. CONCLUSION

OFDM signals are widely assumed to be robust against interference. This has mainly two reasons. The low power spectral density leads to a fast coverage of the interference by thermal noise with increasing distance compared to single-carrier transmission schemes, and the random coding effectively prohibits the emergence of ghost targets. Yet, the interfering energy still defines the noise level in the rv -map and the random coding prohibits robust mitigation strategies in any domain during the evaluation process. Only adaptive digital beamforming, whose OFDM radar specific application is presented, delivers sufficient results. Alternatively, the specific modulation form repeated-symbol OFDM may be used. Although RS-OFDM modulation sounds rather disadvantageous, it actually allows interference-robust processing of OFDM signals. This is achieved by interference shaping towards specific velocity columns, that are outside the region of interest for the radar by use of a small carrier-frequency shift. The concept does not require strict rules for cooperation, and it is possible to modify the modulation parameters during operation. Additionally, the adoptions in modulation domain also allow to apply conventional mitigation strategies in Doppler-domain non-cooperatively. Both concepts lead to a dynamic range that is close to the interference-free case.

REFERENCES

- [1] F. Roos, J. Bechter, C. Knill, B. Schweizer, and C. Waldschmidt, "Radar sensors for autonomous driving: Modulation schemes and interference mitigation," *IEEE Microw. Mag.*, vol. 20, no. 9, pp. 58–72, Sep. 2019, doi: [10.1109/MMM.2019.2922120](https://doi.org/10.1109/MMM.2019.2922120).
- [2] C. Knill, B. Schweizer, P. Hügler, and C. Waldschmidt, "Impact of an automotive chirp-sequence interferer on a wideband OFDM radar," in *Proc. 15th Eur. Radar Conf.*, 2018, pp. 34–37, doi: [10.23919/EuRAD.2018.8546524](https://doi.org/10.23919/EuRAD.2018.8546524).
- [3] B. Nuss, L. Sit, and T. Zwick, "A novel technique for interference mitigation in OFDM radar using compressed sensing," in *Proc. IEEE MTT-S Int. Conf. Microw. Intell. Mobility*, 2017, pp. 143–146, doi: [10.1109/ICMIM.2017.7918877](https://doi.org/10.1109/ICMIM.2017.7918877).
- [4] C. Knill, B. Schweizer, and C. Waldschmidt, "Interference-robust processing of OFDM radar signals using compressed sensing," *IEEE Sens. Lett.*, vol. 4, no. 4, pp. 1–4, Apr. 2020, Art no. 7001104, doi: [10.1109/LSSENS.2020.2980165](https://doi.org/10.1109/LSSENS.2020.2980165).
- [5] G. Hakobyan and B. Yang, "A novel narrowband interference suppression method for OFDM radar," in *Proc. Eur. Signal. Process. Conf.*, 2016, pp. 2230–2234, doi: [10.1109/EUSIPCO.2016.7760645](https://doi.org/10.1109/EUSIPCO.2016.7760645).
- [6] C. Knill, J. Bechter, and C. Waldschmidt, "Interference of chirp sequence radars by OFDM radars at 77 GHz," in *Proc. IEEE MTT-S Int. Conf. Microw. Intell. Mobility*, 2017, pp. 147–150, doi: [10.1109/ICMIM.2017.7918878](https://doi.org/10.1109/ICMIM.2017.7918878).
- [7] S. Alland, W. Stark, M. Ali, and M. Hegde, "Interference in automotive radar systems: Characteristics, mitigation techniques, and current and future research," *IEEE Signal Process. Mag.*, vol. 36, no. 5, pp. 45–59, Sep. 2019, doi: [10.1109/MSP.2019.2908214](https://doi.org/10.1109/MSP.2019.2908214).
- [8] G. K. Carvajal et al., "Comparison of automotive FMCW and OFDM radar under interference," in *Proc. IEEE Radar Conf. (RadarConf20)*, 2020, pp. 1–6, doi: [10.1109/RadarConf2043947.2020.9266449](https://doi.org/10.1109/RadarConf2043947.2020.9266449).
- [9] J. Overvest, F. Laghezza, F. Jansen, and A. Filippi, "Radar waveform coexistence: Interference comparison on multiple-frame basis," in *Proc. 17th Eur. Radar Conf.*, 2021, pp. 168–171, doi: [10.1109/EuRAD48048.2021.00052](https://doi.org/10.1109/EuRAD48048.2021.00052).
- [10] Y. L. Sit and T. Zwick, "MIMO OFDM radar with communication and interference cancellation features," in *Proc. IEEE Radar Conf.*, 2014, pp. 265–268, doi: [10.1109/RADAR.2014.6875596](https://doi.org/10.1109/RADAR.2014.6875596).
- [11] C. Aydogdu et al., "Radar interference mitigation for automated driving: Exploring proactive strategies," *IEEE Signal Process. Mag.*, vol. 37, no. 4, pp. 72–84, Jul. 2020, doi: [10.1109/MSP.2020.2969319](https://doi.org/10.1109/MSP.2020.2969319).
- [12] G. Hakobyan, K. Armanious, and B. Yang, "Interference-aware cognitive radar: A remedy to the automotive interference problem," *IEEE Trans. Aerosp. Electron. Syst.*, vol. 56, no. 3, pp. 2326–2339, Jun. 2020, doi: [10.1109/TAES.2019.2947973](https://doi.org/10.1109/TAES.2019.2947973).
- [13] C. Sturm and W. Wiesbeck, "Waveform design and signal processing aspects for fusion of wireless communications and radar sensing," *Proc. IEEE*, vol. 99, no. 7, pp. 1236–1259, Jul. 2011, doi: [10.1109/JPROC.2011.2131110](https://doi.org/10.1109/JPROC.2011.2131110).
- [14] E. Mozeson and N. Levanon, "Multicarrier radar signals with low peak-to-mean envelope power ratio," *IEE Proc. Radar, Sonar, Navigat.*, vol. 150, no. 2, pp. 71–77, 2003, doi: [10.1049/ip-rsn:20030263](https://doi.org/10.1049/ip-rsn:20030263).
- [15] A. Bourdoux, M. Bauduin, and C. Desset, "IQ imbalance robust and low PAPR OFDM radar waveform," in *Proc. IEEE Radar Conf.*, 2019, pp. 1–6, doi: [10.1109/RADAR.2019.8835496](https://doi.org/10.1109/RADAR.2019.8835496).
- [16] B. Schweizer, C. Knill, D. Schindler, and C. Waldschmidt, "Stepped-carrier OFDM-radar processing scheme to retrieve high-resolution range-velocity profile at low sampling rate," *IEEE Trans. Microw. Theory Techn.*, vol. 66, no. 3, pp. 1610–1618, Mar. 2017, doi: [10.1109/TMTT.2017.2751463](https://doi.org/10.1109/TMTT.2017.2751463).
- [17] B. Schweizer et al., "The fairy tale of simple all-digital radars: How to deal with 100 gbit/s of a digital millimeter-wave MIMO radar on an FPGA," *IEEE Microw. Mag.*, vol. 22, no. 7, pp. 66–76, Jul. 2021, doi: [10.1109/MMM.2021.3069602](https://doi.org/10.1109/MMM.2021.3069602).
- [18] B. Farley, J. McGrath, and C. Erdmann, "An all-programmable 16-nm RFSoc for digital-RF communications," *IEEE Micro*, vol. 38, no. 2, pp. 61–71, Mar. 2018, doi: [10.1109/MM.2018.022071136](https://doi.org/10.1109/MM.2018.022071136).
- [19] M. Kucharski, A. Ergintav, W. A. Ahmad, M. Krstić, H. J. Ng, and D. Kissinger, "A scalable 79-GHz radar platform based on single-channel transceivers," *IEEE Trans. Microw. Theory Techn.*, vol. 67, no. 9, pp. 3882–3896, Sep. 2019, doi: [10.1109/TMTT.2019.2914104](https://doi.org/10.1109/TMTT.2019.2914104).

- [20] C. Vasanelli, R. Batra, A. D. Serio, F. Boegelsack, and C. Waldschmidt, "Assessment of a millimeter-wave antenna system for MIMO radar applications," *IEEE Antennas Wireless Propag. Lett.*, vol. 16, pp. 1261–1264, 2017, doi: [10.1109/LAWP.2016.2631889](https://doi.org/10.1109/LAWP.2016.2631889)
- [21] H. Urkowitz, "Energy detection of a random process in colored gaussian noise," *IEEE Trans. Aerosp. Electron. Syst.*, vol. AES- 5, no. 2, pp. 156–162, Mar. 1969, doi: [10.1109/TAES.1969.309901](https://doi.org/10.1109/TAES.1969.309901).
- [22] C. Sturm, E. Pancera, T. Zwick, and W. Wiesbeck, "A novel approach to OFDM radar processing," in *Proc. IEEE Radar Conf.*, 2009, pp. 1–4, doi: [10.1109/RADAR.2009.4977002](https://doi.org/10.1109/RADAR.2009.4977002).
- [23] C. Sturm, M. Braun, T. Zwick, and W. Wiesbeck, "A multiple target doppler estimation algorithm for OFDM based intelligent radar systems," in *Proc. 7th Eur. Radar Conf.*, 2010, pp. 73–76.
- [24] C. Knill, F. Embacher, B. Schweizer, S. Stephany, and C. Waldschmidt, "Coded OFDM waveforms for MIMO radars," *IEEE Trans. Veh. Technol.*, pp. 1–1, 2021, doi: [10.1109/TVT.2021.3073268](https://doi.org/10.1109/TVT.2021.3073268).
- [25] J. Bechter and C. Waldschmidt, "Automotive radar interference mitigation by reconstruction and cancellation of interference component," in *Proc. IEEE MTT-S Int. Conf. Microw. Intell. Mobility*, 2015, pp. 1–4, doi: [10.1109/ICMIM.2015.7117954](https://doi.org/10.1109/ICMIM.2015.7117954).
- [26] J. Bechter, K. D. Biswas, and C. Waldschmidt, "Estimation and cancellation of interferences in automotive radar signals," in *Proc. 18th Int. Radar Symp.*, 2017, pp. 1–10, doi: [10.23919/IRS.2017.8008126](https://doi.org/10.23919/IRS.2017.8008126).
- [27] F. Uysal and S. Sanka, "Mitigation of automotive radar interference," in *Proc. IEEE Radar Conf.*, 2018, pp. 0405–0410, doi: [10.1109/RADAR.2018.8378593](https://doi.org/10.1109/RADAR.2018.8378593).
- [28] B. D. Van Veen and K. M. Buckley, "Beamforming: A versatile approach to spatial filtering," *IEEE Acoust., Speech, Signal Process. Mag.*, vol. 5, no. 2, pp. 4–24, Apr. 1988, doi: [10.1109/53.665](https://doi.org/10.1109/53.665).
- [29] J. Bechter, K. Eid, F. Roos, and C. Waldschmidt, "Digital beamforming to mitigate automotive radar interference," in *Proc. IEEE MTT-S Int. Conf. Microw. Intell. Mobility*, 2016, pp. 1–4, doi: [10.1109/ICMIM.2016.7533914](https://doi.org/10.1109/ICMIM.2016.7533914).
- [30] J. Bechter, M. Rameez, and C. Waldschmidt, "Analytical and experimental investigations on mitigation of interference in a DBF MIMO radar," *IEEE Trans. Microw. Theory Techn.*, vol. 65, no. 5, pp. 1727–1734, May 2017, doi: [10.1109/TMTT.2017.2668404](https://doi.org/10.1109/TMTT.2017.2668404).
- [31] B. Widrow, P. E. Mantey, L. J. Griffiths, and B. B. Goode, "Adaptive antenna systems," *Proc. IEEE*, vol. 55, no. 12, pp. 2143–2159, Dec. 1967, doi: [10.1109/PROC.1967.6092](https://doi.org/10.1109/PROC.1967.6092).
- [32] J. Bechter, A. Demirlika, P. Hügler, F. Roos, and C. Waldschmidt, "Blind adaptive beamforming for automotive radar interference suppression," in *Proc. 19th Int. Radar Symp.*, 2018, pp. 1–10, doi: [10.23919/IRS.2018.8447965](https://doi.org/10.23919/IRS.2018.8447965).
- [33] R. Gooch and J. Lundell, "The CM array: An adaptive beamformer for constant modulus signals," in *Proc. IEEE Int. Conf. Acoust., Speech, Signal Process.*, vol. 11, 1986, pp. 2523–2526, doi: [10.1109/ICASSP.1986.1168686](https://doi.org/10.1109/ICASSP.1986.1168686).
- [34] J. Treichler and B. Agee, "A new approach to multipath correction of constant modulus signals," *IEEE Trans. Acoust., Speech, Signal Process.*, vol. 31, no. 2, pp. 459–472, Apr. 1983, doi: [10.1109/TASSP.1983.1164062](https://doi.org/10.1109/TASSP.1983.1164062).
- [35] V. Venkataraman, R. E. Cagley, and J. J. Shynk, "Adaptive beamforming for interference rejection in an OFDM system," in *Proc. 37th Asilomar Conf. Signals, Syst., Comput.*, vol. 1, Nov. 2003, pp. 507–511, doi: [10.1109/ACSSC.2003.1291962](https://doi.org/10.1109/ACSSC.2003.1291962).
- [36] G. Hakobyan, M. Girma, X. Li, N. Tammireddy, and B. Yang, "Repeated symbols OFDM-MIMO radar at 24 GHz," in *Proc. Eur. Radar Conf.*, 2016, pp. 249–252.
- [37] G. Franken, H. Nikoogar, and P. van Genderen, "Doppler tolerance of OFDM-coded radar signals," in *Proc. Eur. Radar Conf.*, 2006, pp. 108–111, doi: [10.1109/EURAD.2006.280285](https://doi.org/10.1109/EURAD.2006.280285).
- [38] W. Soergel, T. Poguntke, and T. Binzer, "IMIKO-radar: Methods for cooperative interference mitigation," presented at Automot. Forum, Eur. Microw. Week 2020, Utrecht, Netherlands, 2021.
- [39] A. Demir, A. Mehrotra, and J. Roychowdhury, "Phase noise in oscillators: A unifying theory and numerical methods for characterization," *IEEE Trans. Circuits Syst. I, Fundam. Theory Appl.*, vol. 47, no. 5, pp. 655–674, May 2000, doi: [10.1109/81.847872](https://doi.org/10.1109/81.847872).
- [40] A. Frischen, J. Hasch, and C. Waldschmidt, "Performance degradation in cooperative radar sensor systems due to uncorrelated phase noise," in *Proc. 11th Eur. Radar Conf.*, 2014, pp. 241–244, doi: [10.1109/EuRAD.2014.6991252](https://doi.org/10.1109/EuRAD.2014.6991252).



Young Engineer Prize in 2018.



BENEDIKT SCHWEIZER (Graduate Student Member, IEEE) received the M.Sc. degree in electrical engineering from Ulm University, Ulm, Germany, in 2016.

From 2014 to 2015, he interned with Robert Bosch Research and Technology Center, Palo Alto, CA, USA. In 2016, he joined the Institute of Microwave Engineering, Ulm University, where he is currently working toward the Ph.D. degree with his research focus on digital radar systems.

Mr. Schweizer was the recipient of the EuRAD

CHRISTINA KNILL (Graduate Student Member, IEEE) received the M.Sc. degree in electrical engineering from Ulm University, Ulm, Germany, in 2015, where she is currently working toward the Ph.D. degree.

In 2015, she joined the Institute of Microwave Engineering, Ulm University. Her research interests include digital signal processing of OFDM radars for future adaptive radar sensors and novel digital radar signal processing methods.

DAVID WERBUNAT (Graduate Student Member, IEEE) received the M.Sc. degree in electrical engineering from Ulm University, Ulm, Germany, in 2019, where he is currently working toward the Ph.D. degree with the Institute of Microwave Engineering.

His current research interests include digital radar systems and also system concepts and signal processing for coherent radar networks.

SIMON STEPHANY received the M.Sc. degree in electrical engineering from Ulm University, Ulm, Germany, in 2018, where he is currently working toward the Ph.D. degree.

In 2018, he joined the Institute of Microwave Engineering, Ulm University. His current research interests include digital circuit design, hardware implementations of digital radars, and passive radar concepts.

CHRISTIAN WALDSCHMIDT (Senior Member, IEEE) received the Dipl.-Ing. (M.S.E.E.) and the Dr.-Ing. (Ph.D.E.E.) degrees from the University Karlsruhe, Karlsruhe, Germany, in 2001 and 2004, respectively. From 2001 to 2004, he was a Research Assistant with the Institut für Höchstfrequenztechnik und Elektronik, Universität Karlsruhe, Germany. Since 2004, he has been with Robert Bosch GmbH, in the business units Corporate Research and Chassis Systems. He was heading different research and development teams in

microwave engineering, RF-sensing, and automotive radar. In 2013, he returned to academia. He was appointed as the Director of the Institute of Microwave Engineering, Ulm University, Ulm, Germany, as Full Professor. He authored or coauthored more than 200 scientific publications and more than 20 patents. His research interests include radar and RF-sensing, mm-wave and submillimeter-wave engineering, antennas and antenna arrays, rf, and array signal processing.

Prof. Waldschmidt is currently a member of the Executive Committee Board of the German MTT/AP joint chapter, and a member of the German Information Technology Society (ITG). He is the Chair of the IEEE MTT-29 Technical Committee on Microwave Aerospace Systems and served as the Chair of MTT-27 Technical Committee on Wireless Enabled Automotive and Vehicular Applications. He was the two-time TPC Chair and General Chair of the IEEE MTT International Conference on Microwaves for Intelligent Mobility. Since 2018, he has been an Associate Editor for IEEE MICROWAVE WIRELESS COMPONENTS LETTERS. He is a reviewer for multiple IEEE transactions and many IEEE conferences in the field of microwaves. He was the co-recipient of 11 best paper awards since 2014.